




Cite this: DOI: 10.1039/c8nj02011f

A multi-responsive thiosemicarbazone-based probe for detection and discrimination of group 12 metal ions and its application in logic gates†

Soma Sarkar, Tapashree Mondal, Swapnadip Roy, Rajnarayan Saha,
Ashish Kumar Ghosh‡ and Sujit S. Panja *

A new simple 3-in-1 multi-response thiosemicarbazone-based chemosensor has been synthesized and characterized. The probe not only exhibited high sensitivity towards the most familiar and abundant group 12 metal ions, viz., Zn^{2+} , Cd^{2+} and Hg^{2+} , in $\text{MeCN-H}_2\text{O}$ (1:1, v/v) medium but also can efficiently distinguish them through significant changes in their absorption and emission spectral behavior. The selectivity response was found to follow the order Hg^{2+} , Cd^{2+} , Zn^{2+} due to the different degrees of stability of their respective complexes, which was further established by TDDFT calculations and interference studies. The binding affinities of the probe towards these metal ions were investigated by absorption, fluorescence emission, fluorescence lifetime, mass spectral and ^1H NMR spectral measurements. The effects of solvent polarity on the probe molecule were also examined. Due to the observation of different binding affinities and the ensuing significant changes in absorbance at different wavelengths by a combination of different inputs, **L** can be judiciously applied for the construction of some basic logic gates (AND, OR, NOT, IMPLICATION and INHIBIT).

Received 25th April 2018,
Accepted 3rd August 2018

DOI: 10.1039/c8nj02011f

rsc.li/njc

Introduction

With the increasing growth of mining and industry over the past decades, heavy metal ion pollution has become a major global problem because many of these metal ions are highly toxic and adversely affect human health and the environment. Hence, over the last few decades, selective and sensitive recognition of heavy transition metal ions has drawn intense attention due to increasing concerns about human health and environmental safety.¹ Additionally, some heavy and transition metal ions are highly crucial to the lives of organisms.² In biological systems, zinc, cadmium and mercury play distinct roles, although they belong to the same group of the periodic table (group 12) and thus exhibit similar electronic configurations and chemical properties. In the human body, zinc is the second most abundant micronutrient behind iron. Zinc ion (Zn^{2+}) serves as an essential ingredient for various enzymes and is essential in neural signal transmission, gene transcription and apoptosis.³ Its deficiency causes the genetic autosomal disorder enteropathica;⁴ moreover, imbalance of zinc metabolism may lead to

numerous health problems, such as superficial skin disease, diabetes, prostate cancer, Alzheimer's disease, and Parkinson's disease.⁵ Cadmium is a highly toxic and carcinogenic metal. In the list of top twenty hazardous substances reported by the Agency for Toxic Substances and Disease Registry and USEPA, cadmium ranks seventh.⁶ It is extensively used in industry in Ni–Cd batteries, electroplated steel, and ceramic enamels and is used in agriculture in phosphate fertilizers.⁷ Cadmium can cause acute and chronic toxicity to kidneys, lungs, bone and the nervous system by inducing calcium metabolism disorders and renal dysfunction and can cause several other diseases, such as pneumonitis and pulmonary edema; it also increases the possibility of certain types of cancer.⁸ Moreover, mercury is one of the most harmful and extremely hazardous metals. Both the ionic and elemental forms of mercury can be converted by microorganisms into organic methylmercury, which is mostly absorbed into the human body through a daily diet of fish.^{9,10} Exposure to Hg causes a wide array of diseases, viz., arrhythmia, cardiomyopathy, neurological disorders, Minamata disease, prenatal brain damage and gastric disorders.¹¹ Among various important transition metal ions, Zn^{2+} , Cd^{2+} and Hg^{2+} all are relatively significant environmental pollutants. In biosystems, the accumulation of these ions in excess amounts can cause a series of severe diseases and can ultimately lead to lethal consequences.¹² Therefore, the development of fluorescent sensors for selective and sensitive recognition of these ions is of crucial importance.

Department of Chemistry, National Institute of Technology Durgapur, WB, 713209, India. E-mail: sujit.panja@gmail.com; Tel: +91-9474914282

† Electronic supplementary information (ESI) available. See DOI: 10.1039/c8nj02011f

‡ Central Institute of Mining and Fuel Research, Dhanbad 828 108, India.

Currently, developing fluorescent sensors of heavy and transition metal ions remains an active research topic in the environmental, biology and medicinal chemistry fields due to the prospective applications of these sensors in molecular catalysis, biological fluorescence imaging and environmental detection.¹³ A fluorescence chemosensor is a device which senses analytes with fluorescent signal transduction. Compared to fluorescent sensors, colorimetric sensors formed by the combination of a chromophore and receptor unit have attracted much interest because naked-eye detection is a very simple, rapid and inexpensive process to obtain qualitative information.¹⁴

Moreover, the design of a versatile sensor with multiple binding sites that exhibits different colorimetric or fluorescence responses for various analytes can be applied to detect more than one analyte simultaneously. In this regard, multi-analyte sensors have been developed.¹⁵ Recently, some thiosemicarbazone compounds have been constructed as multi-analyte sensors due to their properties of chelate formation with the analytes.¹⁶ Also, thiosemicarbazide compounds and their transition metal complexes have aroused significant interest due to their bioinorganic and pharmacological activities. When the thiosemicarbazide is connected to an N-heterocyclic compound, the ring N atom becomes a strong electron pair donor to form coordination compounds with transition metals.¹⁷ In the neutral form, thiosemicarbazones behave as N–N–S tridentate chelators towards transition metal ions; these N₂S chelated ligand–metal complexes have received considerable interest.¹⁸ Again, for sensing, the system must contain a fluorophore as the signaling moiety. Among various fluorophores, pyrene is an effective fluorescent probe due to its chemical stability, high fluorescence quantum yield, long fluorescence lifetime and monomer–excimer dual emission properties.¹⁹ A variety of multi-ion sensors have been constructed; however, no pyrene derivative has been reported as a sensor for Zn²⁺, Cd²⁺ and Hg²⁺ ions simultaneously. Therefore, it is essential to develop a pyrene-based visual sensor and fluorescent sensor for sensitive detection of these group 12 elements.

In the field of information technology, molecular logic gates have gained much attention for molecular-level information processing due to their ability to provide information at the molecular scale.²⁰ In this field, to execute a useful estimation, the switching process should be a reversible and reproducible chemical process. A truth table has been constructed by following the principles of binary logic function using a few basic logic operations; AND, OR, NOT, XOR, NAND, INHIBIT, *etc.* INHIBIT logic systems are receiving the most interest due to their non-commutative and nonassociative behaviour, *i.e.*, a single input can stop the entire system. A receptor that has different affinities and is associated with different optical outputs in terms of wavelength and intensity toward various metal ions due to multiple binding modes is predicted to carry out simple and integrated logic operations. Hence, molecules containing different coordination sites for a combination of ions or a specific ion are being designed for use as potential molecular operators.²¹

Combining all these concepts in our consideration, we have designed and synthesized a simple 3-in-1 multi-responsive

chemosensor using pyrene as a fluorophore and pyridine thiosemicarbazone as an ionophore to construct a small organic Schiff base-type molecule (**L**) for multi-ion analysis. Furthermore, Schiff bases can be easily prepared and can be applied to optical sensors due to their excellent spectroscopic responses.²² Here, we report the synthesis, characterization and fluorimetric and colorimetric recognition properties of a probe containing N₂S donor atoms to selectively bind the most familiar and abundant group 12 metal ions, *viz.*, Zn²⁺, Cd²⁺ and Hg²⁺, at trace levels. To the best of our knowledge, this is the first pyrene-based chemosensor that can detect these metal ions simultaneously. The selectivity response was found to follow the order of Hg²⁺, Cd²⁺, Zn²⁺. Based on its absorption spectral responses and reversible and reproducible characteristics, the unique receptor **L** can mimic composite logic operations (OR, AND, NOT, INHIBIT and IMPLICATION) by influencing a specific set of inputs in a systematic way. Computational studies employing time-dependent density functional theory (TD-DFT) were performed to further elucidate the experimental results.

Experimental

Materials

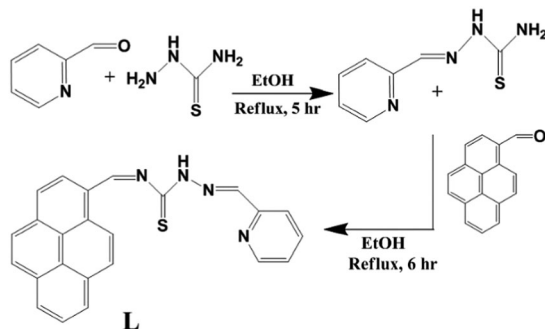
The starting materials (chemical reagents and solvents) were of analytical grade and were obtained from commercial sources. Pyrene-1-carboxaldehyde, pyridine-2-carboxaldehyde and thiosemicarbazide were purchased from Sigma-Aldrich Chemical Company. Solvents such as ethanol, acetonitrile, and diethyl ether were of HPLC grade and were used without further purification. The metal salts were purchased from Merck (India). Deionized water (distilled) was used throughout the experiments.

Apparatus

Absorbance spectra were measured with a Shimadzu UV-1800 Spectrophotometer. All fluorescence measurements were performed with a Hitachi F-2500 Spectrofluorimeter using a 1 cm quartz cuvette with a slit width of 2.5 nm and a scan speed of 5 nm s^{−1}. The PMT voltage of the fluorimeter was maintained at 700 V. pH measurements were conducted with a Eutech Instruments digital pH meter (model pH2100). Proton nuclear magnetic resonance (¹H NMR) spectra of the probe and its Hg-complex were recorded on a Bruker DPX 300 MHz spectrometer in CDCl₃ solution at room temperature with TMS as the internal standard. The mass spectra were acquired on a Micro-mass Q-TOF microTM instrument under ESI mode. The infrared spectrum was recorded on a Thermo Nicolet iS10 spectrophotometer in the range of 4000 to 400 cm^{−1} using KBr pellets. Time-resolved fluorescence lifetimes were measured by time-correlated single photon counting (TCSPC) using a Horiba DeltaFlex™ instrument. The structures of the probe and its metal complexes were optimized by TD-DFT using Gaussian 09 software.

Synthesis and characterization

The Schiff base structure of probe **L** was obtained by a 2 step condensation reaction in satisfactory yield (Scheme 1). In the



Scheme 1 Synthesis of receptor L.

first step, 2 mmol solid thiosemicarbazide (0.18226 gm) was added to an ethanolic solution of pyridine-2-aldehyde (0.2142 gm, 2 mmol). The mixture was refluxed for 5 h, then cooled. After evaporating the solvent under reduced pressure, a yellowish white precipitate appeared; it was washed several times with ethanol and dried under vacuum to afford the pure solid of pyridine thiosemicarbazone. The yield was 76.75%. Then, in the second step, 1 mmol pyridine thiosemicarbazone was added to a hot ethanolic solution of pyrene-1-carboxaldehyde (1 mmol). The resulting bright yellowish solution was refluxed for 6 h, then cooled to room temperature. After evaporating the solvent under vacuum, a light yellow solid was precipitated. The solid was washed with ether several times and dried; the final product (**L**) was obtained in 71.8% yield. FTIR/cm⁻¹ (KBr) ν : 1610 (C=N), 3160 (N-H) (ESI,[†] Fig. S1). ¹H NMR (300 MHz, CHCl₃-d): 9.138 (s, 1H, NH), 8.646 (s, 1H, CH=N), 8.421 (s, 1H, CH=N), 7.98–7.94 (m, 2H, pyrenyl-H), 7.87–7.84 (m, 4H, pyrenyl-H), 7.78–7.74 (m, 3H, pyrenyl-H), 7.34–7.31 (m, 4H, pyridyl-H) (ESI,[†] Fig. S2). ESI MS: 392.5 (**L**) and 393.5 (**L**-H⁺) (ESI,[†] Fig. S3).

Measurement procedures

Because the receptor **L** is not soluble in water, all the experiments were carried out in a MeCN/H₂O (1:1, v/v) solvent mixture. First, a 25×10^{-5} M stock solution of **L** was prepared in the solvent mixture. The stock solutions of Ag⁺, Co²⁺, Pb²⁺, Cr³⁺, Zn²⁺, Ca²⁺, Na⁺, Cu²⁺, Mn²⁺, Ni²⁺, Cd²⁺, Hg²⁺ and Fe³⁺ (1 mM) were obtained by dissolving their metal chloride salts in the solvent mixture (MeCN/H₂O, 1:1). Before each absorption or fluorescence measurement, the solutions were allowed to stand for 10 min to complete the formation of the metal–ligand complex. A wide pH range of Tris–HCl buffered solutions of **L** (25 μ M) in the absence and presence of metal ions, viz., Zn²⁺ (2.5×10^{-4} M), Cd²⁺ (2.5×10^{-4} M) and Hg²⁺ (2.5×10^{-4} M), was obtained by adjusting the pH with the addition of requisite amounts of HCl or NaOH solution.

Results and discussion

Visual colorimetric analysis

In the absence of metal ions, the MeCN/aqueous (1:1, v/v) solution of the ligand (**L**) was colorless. When a solution of **L**

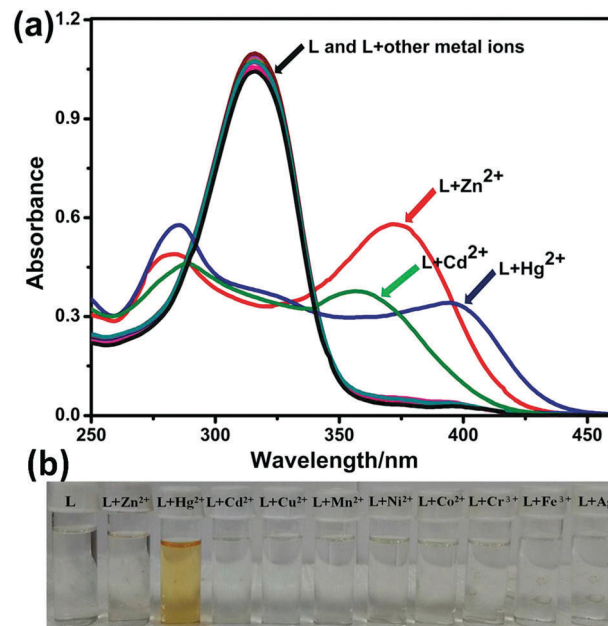


Fig. 1 (a) Absorption spectra and (b) colour changes of probe **L** (2.5×10^{-5} M) with various metal ions (4 equiv. each) in Tris buffered MeCN/H₂O (1:1, v/v, pH 7) solution.

was treated with various metal ions, a remarkable color change from colorless to yellow was noted for Hg²⁺ only (Fig. 1b). The addition of several other metal ions (e.g., Fe³⁺, Cr³⁺, Ag⁺, Zn²⁺, Cd²⁺, Mn²⁺, Ni²⁺, Co²⁺, Cu²⁺) did not exhibit any detectable color change. This observation can easily be elucidated by the presence of the extended tail in the visible region in the electromagnetic spectrum, as seen in the absorption spectrum for Hg²⁺. This result indicates that **L** can be used as a highly selective naked-eye sensor for Hg²⁺ ion. This colorimetric recognition toward various metal ions was further demonstrated by UV-Visible and fluorimetric methods.

Absorption studies

In order to investigate the sensing properties of chemosensor **L** toward various metal ions, it was necessary to select a suitable solvent. Hence, the absorption spectra of **L** were recorded in different solvents (THF, DMF, DMSO, MeCN, EtOH and MeOH). As shown in the ESI,[†] Fig. S7, among the various solvents, the probe displayed the maximum absorbance in MeCN solution. In DMSO, the absorbance of **L** was also high; however, due to the intrinsic coordination and oxidizing properties of DMSO, we chose MeCN medium for the analysis. Further, in 50% aqueous–MeCN solution, appreciable spectra were obtained during the titration with metal ions. For this reason, MeCN/H₂O (1:1, v/v) medium was selected for all the spectroscopic studies. The UV-Vis absorption spectrum of **L** revealed a broad absorption band at around 316 nm in MeCN/aqueous (1:1, v/v) Tris–HCl buffer (10 mM, pH 7) medium, which can be ascribed to the presence of the enlarged conjugated system of the pyrene chromophore unit in the probe. Selectivity is an important and essential requirement for an excellent chemosensor. Therefore,

the selectivity of **L** was tested by the addition of chloride salts of a variety of metal ions: Ag^+ , Cu^{2+} , Fe^{3+} , Cr^{3+} , Mn^{2+} , Hg^{2+} , Ni^{2+} , Co^{2+} , Na^+ , Ca^{2+} , Pb^{2+} , Al^{3+} , Zn^{2+} and Cd^{2+} (Fig. 1a). Addition of only Zn^{2+} , Cd^{2+} and Hg^{2+} ions to **L** produced distinct spectral changes, whereas other metal ions did not significantly influence the spectral properties of **L**. The intensity of the absorption maximum at 316 nm exhibited a significant decrease upon addition of Zn^{2+} , Cd^{2+} and Hg^{2+} along with bathochromic shifts.

To better assess the interactions between **L** and representative metal ions (Zn^{2+} , Cd^{2+} and Hg^{2+}), spectrophotometric titration experiments were performed independently for each metal ion in aqueous MeCN medium (Fig. 2). Progressive addition of Zn^{2+} to **L** resulted in a small band at 280 nm and a new red shifted absorption signal at 373 nm; these signals were gradually enhanced with increasing amount of Zn^{2+} ions, while the intensity of the absorption at 316 nm decreased correspondingly (Fig. 2a). Two distinct isosbestic points appeared at 286 nm and 340 nm. After the addition of more than 1 equiv. of Zn^{2+} , no further change was noted. On successive addition of Cd^{2+} to **L**, a similar trend was observed. There was a gradual decrease of the absorbance at 316 nm and a systematic growth of the absorbance maxima at 357 nm and around 284 nm along with two distinct isosbestic points at 339 nm and 289 nm (Fig. 2b).

Similarly, upon incremental addition of Hg^{2+} ion, disappearance of the absorption peak at 316 nm was also seen, with the appearance of a new peak at 394 nm and a small peak at 286 nm along with two clear isosbestic points at 340 nm and 292 nm (Fig. 2c). In each case, the presence of two well-defined isosbestic points indicates the formation of a stable complex of **L** with the respective metal ions as well as the occurrence of two types of simultaneous electronic transitions originating from the metal complex on both the higher and lower energy side with respect to the transition originating from the ligand itself (at 316 nm). The absorbance at the blue end may be ascribed to the transition from the ground electronic level to the excited electronic state of the ligand in the presence of metal, whereas the absorbance observed at the red end indicates a charge transfer mechanism between the ligand and metal ion. The sigmoidal curves shown in the ESI,† Fig. S8–S10, were obtained by plotting the changes in the maximum absorption intensity as a function of the Zn^{2+} , Cd^{2+} and Hg^{2+} concentration. The most important feature was the shift in the absorbance maximum of **L** from 316 nm to 394 nm ($\Delta\lambda = 78$ nm) after addition of Hg^{2+} ; this shift was 57 nm for Zn^{2+} and 41 nm for Cd^{2+} . This result demonstrates that the probe not only detects three elements in group 12 of the periodic table, but also can easily distinguish Zn^{2+} , Cd^{2+} and Hg^{2+} from other metal ions.

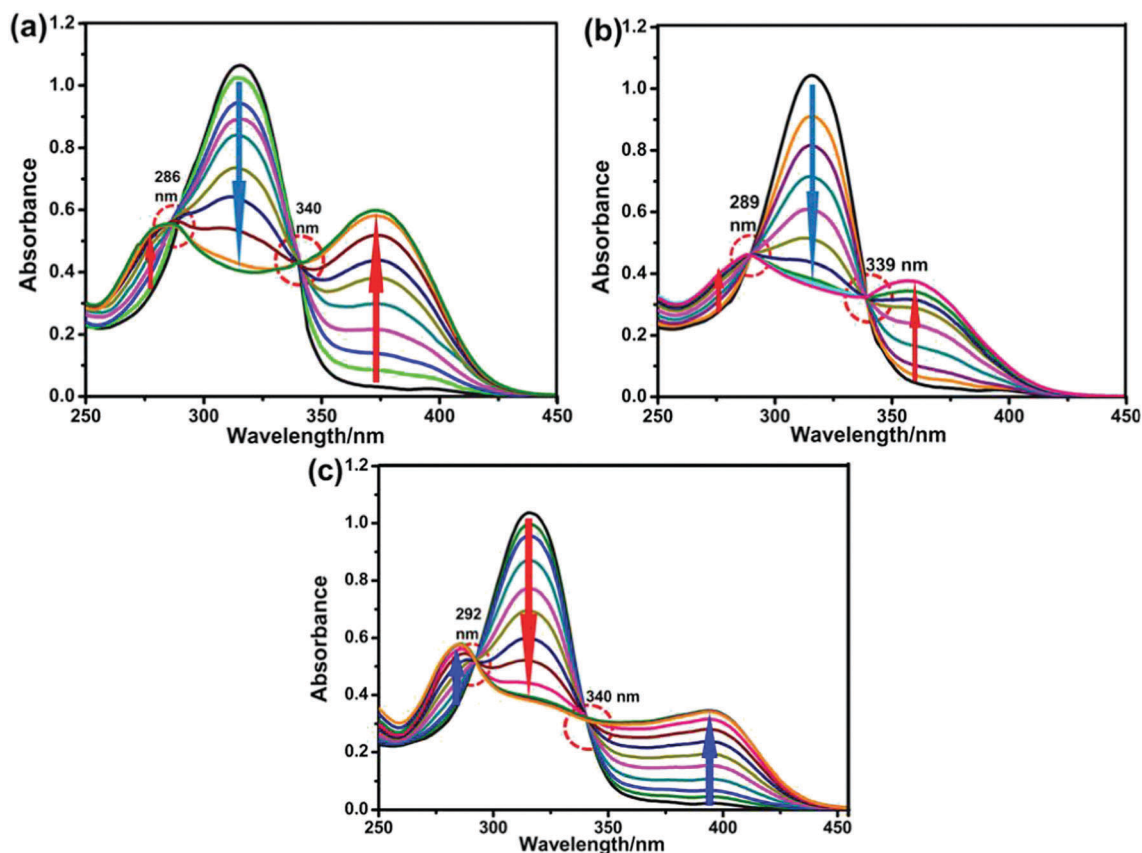


Fig. 2 Spectrophotometric titration spectra of probe **L** (2.5×10^{-5} M) upon addition of (a) Zn^{2+} ion ($[\text{Zn}^{2+}] = 0, 2.5, 5, 7.5, 10, 12.5, 15, 20, 25, 37.5 \mu\text{M}$), (b) Cd^{2+} ion ($[\text{Cd}^{2+}] = 0, 1.25, 2.5, 5, 7.5, 10, 12.5, 15, 20, 25 \mu\text{M}$) and (c) Hg^{2+} ion ($[\text{Hg}^{2+}] = 0, 1.25, 2.5, 5, 7.5, 10, 12.5, 15, 17.5, 20, 22.5, 25 \mu\text{M}$) in Tris buffered MeCN/ H_2O (1:1, v/v, pH 7) solutions.

Emission studies

The changes in the emission properties of the Schiff base ligand (**L**) were also investigated in the presence of these metal ions in MeCN/aqueous (1 : 1, v/v) Tris-HCl buffer (10 mM, pH 7) medium. Upon excitation at 350 nm, the probe **L** displayed a broad emission peak with a maximum intensity at around 452 nm, which is an important characteristic of the pyrene moiety. Fascinatingly, upon treatment of receptor **L** with Zn^{2+} ion, fluorescence quenching was observed. With increasing concentration of Zn^{2+} up to 1 equiv., the intensity of the emission at 452 nm reached a minimum value (Fig. 3a), indicating the formation of a weakly fluorescent [**L**- Zn^{2+}] complex. The quantum yield of the Zn-complex was enumerated to be 0.047, slightly lower (3.2-fold) than that of the isolated ligand ($\Phi_f = 0.149$). A similar trend was noted in the fluorescence emission spectra of **L** when excited at 350 nm and 385 nm, respectively, during titration of **L** with Cd^{2+} and Hg^{2+} ; the emission band at 452 nm linearly decreased up to 1 equiv. of Cd^{2+} ions and 2 equiv. of Hg^{2+} ions (Fig. 3b and c). The calculated quantum yields of the [**L**- Cd^{2+}] and [**L**- Hg^{2+}] complexes were 0.038 and 0.024, respectively, which are 4-fold and 6.2-fold lower than that of receptor **L**. It is known that among the relevant metal ions, Zn^{2+} , Cd^{2+} and Hg^{2+} show high thermodynamic affinities for ligands with N or S donor atoms. Hence, the decrease of emission intensity was ascribed to the introduction of Zn^{2+} , Cd^{2+} or Hg^{2+} and, accordingly, the occurrence of strong complexation with **L** through N and S heteroatoms followed by separation of the intermolecular π -stacked pyrene moieties. The decrease in the excimer intensity was also attributed to the heavy metal effect of these metal ions.

The fluorescence quenching efficiency can be determined by the Stern-Volmer relation:²³ $I_0/I = 1 + K_{SV} [Q]$; from this equation, the quenching constant can be calculated. I_0 and I are the emission intensities in absence of quencher (Q) and the presence of quencher (Q), respectively, K_{SV} is the Stern-Volmer quenching constant and $[Q]$ is the concentration of the quencher. The plot of I_0/I vs. quencher concentration exhibited a linear relationship²⁴ (ESI,† Fig. S11-S13); from these plots, the values of K_{SV} for the Zn^{2+} , Cd^{2+} and Hg^{2+} complexes with **L** were found to be $8.5 \times 10^4 \text{ M}^{-1}$, $9.3 \times 10^4 \text{ M}^{-1}$ and $9.7 \times 10^4 \text{ M}^{-1}$, respectively.

A linear Stern-Volmer plot is generally indicative of a single class of fluorophore; here, the quenching mechanism was predicted to be static in nature, which was further ascertained from the absorption spectra of **L** in the presence of these metal ions, as static quenching is a phenomenon of ground state complex formation.^{13a} The quenching mechanism was also confirmed from time-resolved fluorescence measurements, which will be discussed later.

Effect of pH

To examine the pH sensitivity of **L** in the absence and presence of Zn^{2+} , Cd^{2+} and Hg^{2+} ion, absorption studies were conducted in a pH range from 3 to 12 (Fig. 4). The absorbance at 316 nm of the metal free sensor **L** was slightly weak at low pH but possessed a good response in the pH range of 5 to 12. However, on addition of 1 equivalent of Zn^{2+} , the absorbance at 373 nm remained relatively constant in the entire pH range; this indicated insensitivity to pH and also indicated that the sensor **L** can detect Zn^{2+} over a wide range of pH values from 3 to 12. In the presence of Cd^{2+} and Hg^{2+} ion, **L** did not show any significant change in absorbance at 357 nm and 394 nm, respectively, in the pH range of 6 to 12; this indicates that the probe **L** can be used in the common environmentally and physiologically relevant range of pH 6.0 to 8.0. Hence, all the spectral studies of **L** were performed at pH 7.

Specificity confirmation

The selectivity of a sensor towards a guest in the presence of other competitive species is an important property. Hence, in order to examine the effects of other metal ions on the binding behaviour of **L** with Zn^{2+} , Cd^{2+} and Hg^{2+} , competitive experiments were conducted in MeCN/aqueous medium and monitored by UV-Vis. Consequently, the absorption intensities for Zn^{2+} , Cd^{2+} and Hg^{2+} were investigated at 373 nm, 357 nm and 394 nm, respectively, in the presence of several other metal ions (Mn^{2+} , Cr^{3+} , Ni^{2+} , Co^{2+} , Fe^{3+} , Cu^{2+} , Ag^+ , Na^+ , Ba^{2+} , Pb^{2+} , Fe^{2+} , Al^{3+}) (Fig. 5). As shown in Fig. 5a, in presence of Zn^{2+} , most of the metal ions showed negligible effects on the detection of Zn^{2+} except for Cd^{2+} and Hg^{2+} . After addition of Cd^{2+} to a solution bearing probe **L** and Zn^{2+} , the absorption maximum at

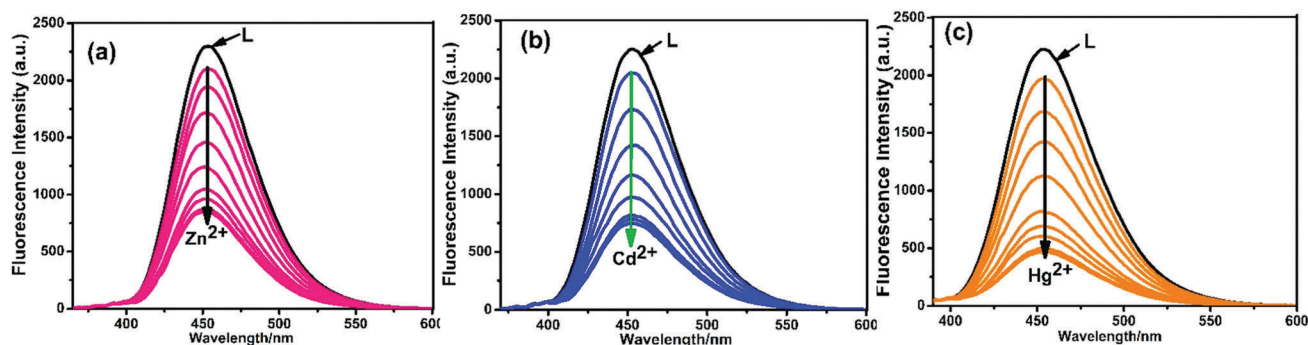


Fig. 3 Fluorescence spectral changes of **L** ($2.5 \times 10^{-5} \text{ M}$) at different concentrations of (a) Zn^{2+} (top to bottom $[\text{Zn}^{2+}] = 0, 1.25, 2.5, 5, 7.5, 10, 12.5, 15, 20, 25, 50 \mu\text{M}$) ($\lambda_{\text{ex}} = 350 \text{ nm}$) (b) Cd^{2+} (top to bottom $[\text{Cd}^{2+}] = 0, 2.5, 5, 7.5, 10, 12.5, 15, 20, 25, 50 \mu\text{M}$) ($\lambda_{\text{ex}} = 350 \text{ nm}$) (c) Hg^{2+} (top to bottom $[\text{Hg}^{2+}] = 0, 2.5, 5, 7.5, 10, 12.5, 15, 17.5, 20, 25, 50 \mu\text{M}$) ($\lambda_{\text{ex}} = 385 \text{ nm}$) in Tris buffered MeCN/ H_2O (1 : 1, v/v, pH 7) solutions.

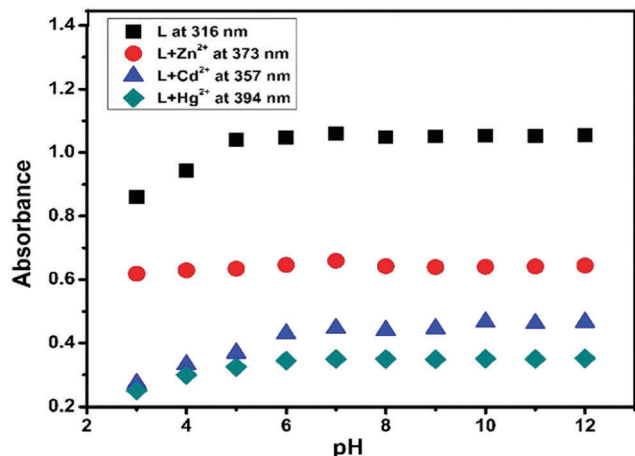


Fig. 4 Effects of pH on the absorbance of **L** at $\lambda_{\text{max}} = 316$ nm, **L** + Zn^{2+} complex at $\lambda_{\text{max}} = 373$ nm, **L** + Cd^{2+} complex at $\lambda_{\text{max}} = 357$ nm and **L** + Hg^{2+} complex at $\lambda_{\text{max}} = 394$ nm.

373 nm caused by Zn^{2+} immediately decreased and readily blue shifted to 357 nm, which is a significant feature of the absorbance caused by Cd^{2+} . Upon addition of Hg^{2+} even at very low concentrations (0.2 equiv.) to a solution of $[\text{L}-\text{Zn}^{2+}]$ adduct, the absorption maximum at 373 nm caused by Zn^{2+} also decreased and red shifted; then, upon gradually adding Hg^{2+} , an absorption band at 394 nm appeared, which is characteristic of the absorbance caused by Hg^{2+} (ESI,† Fig. S14). However, the

competitive experiment for the selectivity of Cd^{2+} verified that the sensing ability of **L** towards Cd^{2+} was not greatly influenced by the presence of most other metal ions but that only Hg^{2+} interfered with the detection of Cd^{2+} by **L** (Fig. 5b). The addition of Hg^{2+} to a solution of $[\text{L}-\text{Cd}^{2+}]$ adduct initially led to a slight decrease and red-shift in the absorbance centered at 357 nm caused by Cd^{2+} ; then, upon gradually adding Hg^{2+} , a new, significantly red-shifted absorption signal centered at 394 nm was observed, which is a characteristic feature of the absorbance caused by Hg^{2+} , as shown in the ESI,† Fig. S15. In contrast, in Fig. 5c, it can be observed that the absorbance exhibited by the mixture of Hg^{2+} with most other metal ions, including Zn^{2+} and Cd^{2+} , was very similar to that caused by Hg^{2+} only, suggesting that the sensing ability of **L** towards Hg^{2+} was not perturbed by other metal ions. These results obviously demonstrate that **L** has stronger binding ability with Hg^{2+} than with Zn^{2+} or Cd^{2+} under the same experimental conditions. The results of the competitive experiments also showed that the sensor **L** can be successfully used for selective detection of Zn^{2+} , Cd^{2+} and Hg^{2+} in the presence of the most relevant competing metal ions. It is also noteworthy that Hg^{2+} can remove Zn^{2+} and Cd^{2+} from their respective metal–ligand complexes, $[\text{L}-\text{Zn}^{2+}]$ and $[\text{L}-\text{Cd}^{2+}]$. Again, Cd^{2+} could remove only Zn^{2+} from the $[\text{L}-\text{Zn}^{2+}]$ complex.²⁵ Very interestingly, this result indicated the stability order of the corresponding metal–ligand complexes to be $[\text{L}-\text{Hg}^{2+}] > [\text{L}-\text{Cd}^{2+}] > [\text{L}-\text{Zn}^{2+}]$. This conclusion was further verified from the binding constant values and theoretical experiments,

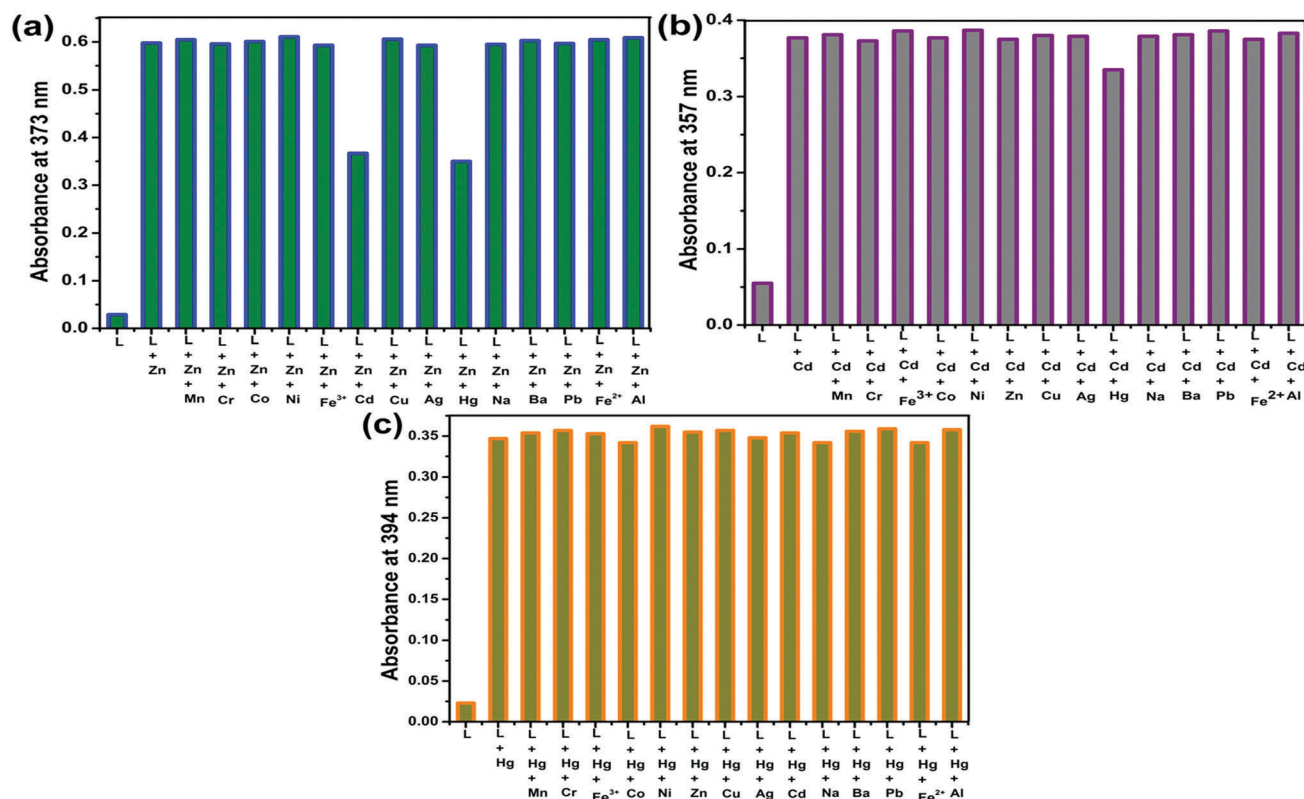
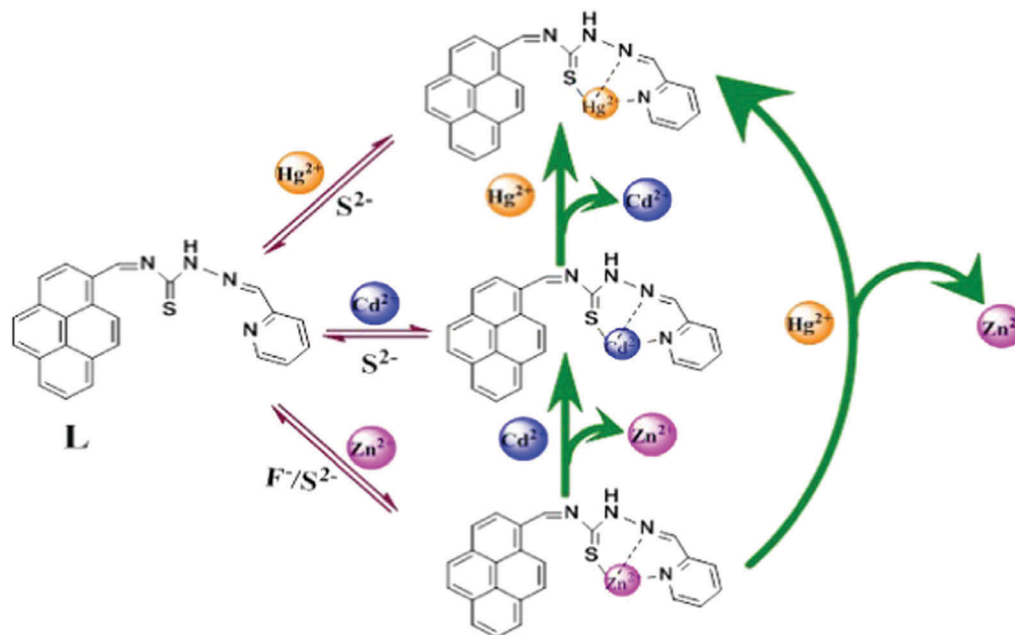


Fig. 5 Variation of the maximum absorbance of **L** (25 μM) with 10 equiv. of other competitive metal ions followed by the addition of 2 equiv. of (a) Zn^{2+} , (b) Cd^{2+} and (c) Hg^{2+} in Tris buffered $\text{MeCN}/\text{H}_2\text{O}$ (1 : 1, v/v, pH 7) solution. ($\lambda_{\text{max}} = 373$ nm for Zn^{2+} , $\lambda_{\text{max}} = 357$ nm for Cd^{2+} and $\lambda_{\text{max}} = 394$ nm for Hg^{2+} .)



Scheme 2 Probable sensing mechanism.

as presented later. The probable competitive sensing abilities of **L** towards Zn^{2+} , Cd^{2+} and Hg^{2+} ions has been nicely shown in a schematic representation (Scheme 2).

Binding stoichiometry, binding constant and detection limit

In order to determine the stoichiometric ratio of **L** with metal ions, a series of solutions of **L**, Zn^{2+} , Cd^{2+} and Hg^{2+} were prepared in Tris HCl containing a MeCN/ H_2O (1 : 1, v/v) solvent mixture. The total concentrations of the resulting solutions remained constant (25 μM). The mole fractions of the externally added metal ions were varied from 0.1 to 1.0. The absorbances at 373 nm for Zn^{2+} , 357 nm for Cd^{2+} and 394 nm for Hg^{2+} were plotted against the mole fractions of the respective metal ions. In the presence of metal ions, the absorbance spectra attained maxima at a mole fraction of 0.5. Job plot analysis (ESI,† Fig. S16) reveals that the binding between the host receptor **L** and the guest metal ions exhibited 1 : 1 binding stoichiometry, which was confirmed by ESI-mass spectrometric analysis (ESI,† Fig. S4–S6). Based on the Benesi–Hildebrand equation,²⁶ the binding constants of **L** with Zn^{2+} , Cd^{2+} and Hg^{2+} were estimated to be $3.125 \times 10^5 \text{ M}^{-1}$, $3.81 \times 10^5 \text{ M}^{-1}$ and $5.58 \times 10^5 \text{ M}^{-1}$, respectively (ESI,† Fig. S17–S19), indicating that $[\text{L}-\text{Hg}^{2+}]$ was the most stable complex and $[\text{L}-\text{Zn}^{2+}]$ was the least stable

complex; this is compatible with the results of the competitive studies. The detection limits (DL) were calculated from the absorption titration profiles of **L** with Zn^{2+} , Cd^{2+} and Hg^{2+} ions on the basis of $3\sigma/K$, where σ is the standard deviation of the blank solution and K is the absolute magnitude of the slope of the calibration curve. The detection limits for Zn^{2+} , Cd^{2+} and Hg^{2+} ions were found to be $1.94 \times 10^{-7} \text{ M}$, $1.57 \times 10^{-7} \text{ M}$ and $1.52 \times 10^{-7} \text{ M}$ (ESI,† Fig. S20–S22), respectively. The results are summarized in Table 1.

Aggregation studies of **L**

The emission properties of pyrene are very sensitive in polar solvents due to the π - π interactions between pyrenyl groups.²⁷ Therefore, the emission spectra of **L** were recorded in MeCN only and MeCN–water binary mixtures containing varied amounts of water (Fig. 6). The fluorescence spectrum of **L** (30 μM) in pure MeCN showed a very poor emission maximum at 413 nm. On increasing the water fraction to 80%, the fluorescence intensity of the excimer sharply increased (~ 65 times) associated with a large red-shift ($\Delta = 50 \text{ nm}$), as shown in the inset (a) of Fig. 6. However, on addition of further water content (up to 90%), the fluorescence intensity decreased bathochromically due to the solubility effect.^{19f} Correspondingly, the quantum yield (Φ) of **L**

Table 1 Spectroscopic and photophysical characteristics of **L** in the absence and presence of Zn^{2+} , Cd^{2+} and Hg^{2+} ions in Tris buffered MeCN/ H_2O (1 : 1, v/v, pH 7) solution

Compound	λ_{abs} (nm)	λ_{em} (nm)	Isosbestic points (nm)	K_{SV} (M^{-1})	K (M^{-1})	DL (M)
L	316	452	—	—	—	—
$[\text{L}-\text{Zn}^{2+}]$ complex	280, 373	452	286, 340	8.5×10^4	3.125×10^5	1.94×10^{-7}
$[\text{L}-\text{Cd}^{2+}]$ complex	284, 357	452	289, 339	9.3×10^4	3.81×10^5	1.57×10^{-7}
$[\text{L}-\text{Hg}^{2+}]$ complex	286, 394	452	292, 340	9.7×10^4	5.58×10^5	1.52×10^{-7}

K_{SV} is the Stern–Volmer quenching constant, K is the binding constant and DL is the limit of detection.

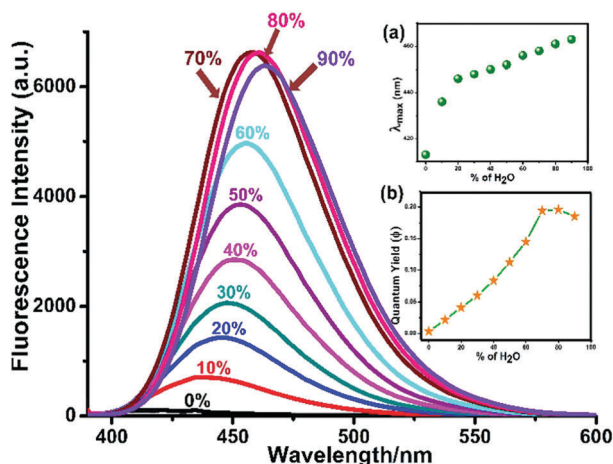


Fig. 6 Effects of water ratio on the fluorescence emission intensity of **L** (30 μ M) (λ_{ex} = 385 nm, slit: 2.5 nm). Inset (a) changes in the wavelength maximum and inset (b) changes in the quantum yield of **L** with varying water fractions (0% to 90%).

was also rapidly enhanced (~ 57.5 times) with increasing water content (0% to 80%) and then decreased, which is shown in the inset (b) of Fig. 6. This sharp enhancement in fluorescence intensity along with a bathochromic shift in the MeCN–water binary mixtures reveals aggregation of **L**, which is ascribed to the aggregation-induced enhanced emission (AIEE) phenomenon²⁸ and the transformation of the excited state from $n-\pi^*$ to $\pi-\pi^*$.²³

¹H NMR studies

To understand the interaction of **L** with Zn^{2+} , Cd^{2+} and Hg^{2+} , ¹H NMR studies were performed independently by adding these metal ions to a $\text{CHCl}_3\text{-d}$ solution of **L** (Fig. 7). Upon addition of 2 equivalents of Zn^{2+} , Cd^{2+} and Hg^{2+} to **L**, significant spectral changes were noted. The peak at 8.421 ppm for the azomethine proton connected with the pyridyl ring was shifted upfield toward 8.389 ppm for Zn^{2+} , 8.361 ppm for Cd^{2+} and 8.332 ppm for Hg^{2+} .

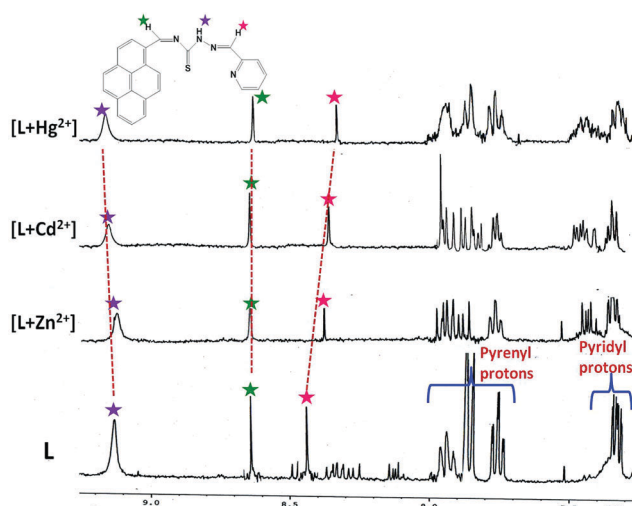


Fig. 7 ¹H NMR spectra of **L** in absence and presence of Zn^{2+} , Cd^{2+} and Hg^{2+} in CDCl_3 .

The proton of the NH group exhibited slight downfield shifts for Zn^{2+} and Cd^{2+} and a downfield shift of 0.06 ppm for Hg^{2+} . Both these shifts indicated strong complexation of $\text{Zn}^{2+}/\text{Cd}^{2+}/\text{Hg}^{2+}$ with the azomethine nitrogen. Further, downfield shifting was observed for the pyridyl ring protons, which suggests the construction of a five-membered ring through the pyridyl N and azomethine N with $\text{Zn}^{2+}/\text{Cd}^{2+}/\text{Hg}^{2+}$ ion. Meanwhile, most of the pyrene protons displayed upfield shifts compared to that of free **L**. These metal ions are soft in nature and prefer to bind soft donors such as S; hence, it is expected that another five-membered ring may be formed through the azomethine N connected to the pyridyl ring and the S of the C=S group with $\text{Zn}^{2+}/\text{Cd}^{2+}/\text{Hg}^{2+}$. Upon addition of Hg^{2+} , the shifting of the protons was greater compared to that when adding Zn^{2+} and Cd^{2+} , indicating the stronger binding ability of **L** with Hg^{2+} ; this is consistent with the results of the competitive studies.

Time-dependent density functional theory (TDDFT) calculations

To determine the theoretical aspects of the observed selective responses of **L** towards Zn^{2+} , Cd^{2+} and Hg^{2+} ions, time-dependent density functional theory (TDDFT) calculations were performed using the Gaussian 09 program. The structures of the compounds were optimized using Becke's three parameters with the Lee–Yang–Parr functional (B3LYP) and a lanl2dz basis set. The energy-optimized stable structures and the probable binding modes of **L** with Zn^{2+} , Cd^{2+} and Hg^{2+} ions are presented in Fig. 8. The contributions of the orbital transitions and their corresponding oscillator strengths are shown in Tables S1 and S2 (ESI[†]). The HOMO–LUMO diagram exhibits that the electron density in the HOMO of **L** is located mainly on the pyridine-thiosemicarbazone moiety, which provides the most binding influence towards metal ions, and that the electron density in the LUMO of **L** is positioned mostly on the pyrene moiety. However, the orbital positions of the HOMO and LUMO in the L-Zn^{2+} , L-Cd^{2+} and L-Hg^{2+} adducts changed due to complexation. The calculated structures show that the corresponding metal ions were perfectly encapsulated into the cavity of **L** by strong electrostatic interactions through the imine-N, pyridyl-N and thiopheno-S atoms of **L**. The corresponding energy values of the individual HOMOs and LUMOs were lower for the complexes compared to that of the free sensor **L** (Table 2), which may be responsible for the red shifts in the UV-Vis absorption spectra upon complexation. The total energies of the complexes were lower in comparison to that of free **L**, indicating higher stability of the complexes. The descending order of the stabilization energy of the complexes is $\text{L-Zn}^{2+} > \text{L-Cd}^{2+} > \text{L-Hg}^{2+}$; hence, the ascending stability order is $\text{L-Zn}^{2+} < \text{L-Cd}^{2+} < \text{L-Hg}^{2+}$. Therefore, the theoretical studies are in good agreement with the experimental observations.

Time-resolved fluorescence studies

Time-resolved fluorescence studies are very important to elucidate the decay processes of the ligand and the complexes. Consequently, the excited state fluorescence lifetimes were measured using 290 nm, 375 nm, 340 nm and 375 nm LED

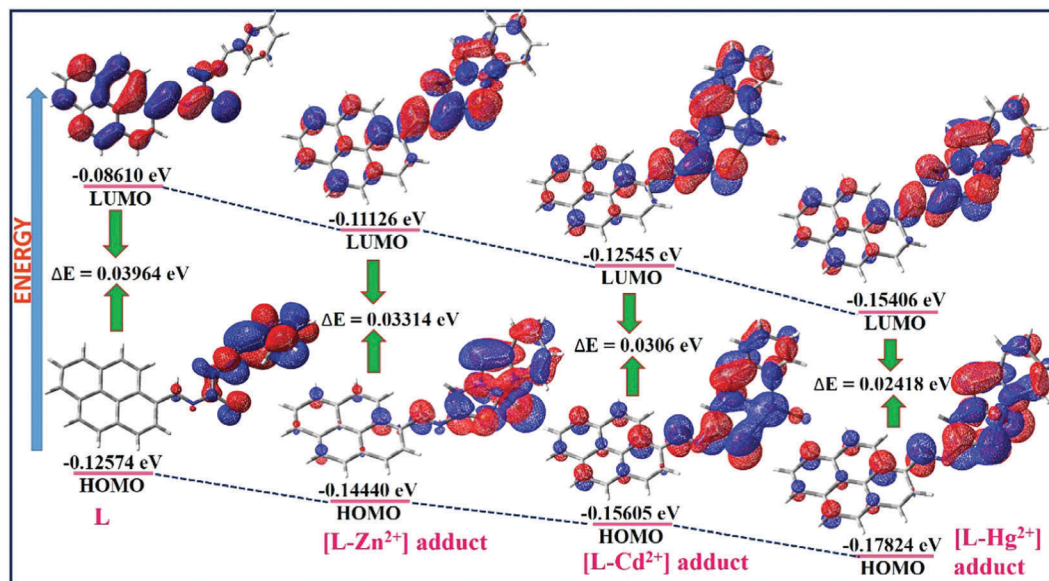


Fig. 8 Frontier molecular orbitals and energy level diagrams of **L** and the [L-Zn²⁺], [L-Cd²⁺] and [L-Hg²⁺] adducts.

Table 2 Comparison of the theoretical energies of **L** in the absence and presence of Zn²⁺, Cd²⁺ and Hg²⁺ ions

Compound	Energy of HOMO (eV)	Energy of LUMO (eV)	ΔE (eV)
L	-0.12574	-0.08610	0.03964
L-Zn²⁺ complex	-0.14440	-0.11126	0.03314
L-Cd²⁺ complex	-0.15605	-0.12545	0.0306
L-Hg²⁺ complex	-0.17824	-0.15406	0.02418

sources for the **L**, **L-Zn²⁺**, **L-Cd²⁺** and **L-Hg²⁺** systems, respectively, while monitoring the emission at 452 nm. The fluorescence lifetime decay plots of **L** and its metal complexes are presented in Fig. 9. The fluorescence lifetime values, quantum yields, and radiative (K_r) and non-radiative (K_{nr}) decay constants of **L** and its corresponding metal complexes are tabulated in Table 3. The radiative and non-radiative decay constants were

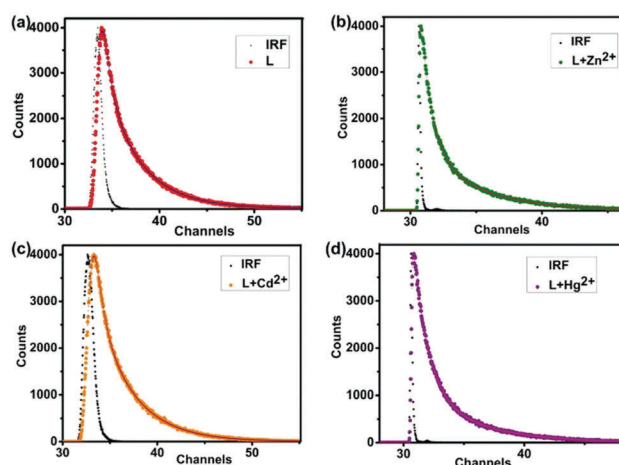


Fig. 9 Changes in the time-resolved fluorescence decay of (a) **L** (λ_{ex} = 290 nm) and the (b) **L-Zn²⁺** (λ_{ex} = 375 nm), (c) **L-Cd²⁺** (λ_{ex} = 340 nm) and (d) **L-Hg²⁺** (λ_{ex} = 375 nm) complexes at λ_{em} = 452 nm.

calculated from the equations: $K_r = \Phi_f/\tau$ and $\tau = 1/(K_r + K_{nr})$. Biexponential fitting was obtained for all the decay processes, and the χ^2 values indicated that this was the best fit for all the decay behaviors. The biexponential decay pattern of the free ligand reflects the presence of a short-lived minor component (0.598 ns, 18.57%) and a long-lived major component (3.79 ns, 81.43%). After complexation of **L** with Zn²⁺, Cd²⁺ and Hg²⁺ ions, the faster decay components (β_1) of **L** were found to increase with a decrease in the values of the longer decay components (β_2), as shown in Table 3. The average fluorescence lifetime values of **L** and the **L-Zn²⁺**, **L-Cd²⁺** and **L-Hg²⁺** complexes were estimated to be 1.9, 1.95, 1.99 and 1.96 ns, respectively. The apparent linear nature of the Stern-Volmer plots alone is not sufficient to reach an unambiguous conclusion regarding whether the mechanism of quenching is dynamic or static in nature. Most of the time, in graphs, the concentration of quencher is taken in an oversimplified way without discriminating the concentrations of free and complexed quencher. Measurement of the fluorescence lifetime is the most definitive method to differentiate between the two mechanisms because we know that for static quenching, $\tau_0/\tau = 1$, whereas for dynamic quenching, $F_0/F = \tau_0/\tau$. The fluorescence lifetime of **L** was found to remain almost identical upon addition of Zn²⁺, Cd²⁺ and Hg²⁺ ions, which further established the *static* nature of the quenching mechanism.^{24a} Notably, the values of K_r and Φ_f of the complexes were lower and the K_{nr} values were higher compared to that of the free ligand. The greater K_{nr} values of the complexes revealed the greater extent of the activities of the nonradiative pathways, resulting in higher quenching of the emission intensity.

Counter ion effect and reusability of **L**

In addition to sensitivity and selectivity, recyclability is a prerequisite to develop a good sensor for practical applications because it determines the cost-effectiveness of real-sample measurements.

Table 3 Fluorescence lifetime decay properties of **L** in the absence and presence of Zn^{2+} , Cd^{2+} and Hg^{2+} ions at $\lambda_{\text{em}} = 452 \text{ nm}$

Compound	τ (ns)	β (%)	$\langle\tau\rangle$ (ns)	χ^2	Φ_f	K_r (10^9 s^{-1})	K_{nr} (10^9 s^{-1})
L	$\tau_1 = 0.598$ $\tau_2 = 3.79$	$\beta_1 = 18.57$ $\beta_2 = 81.43$	1.9	1.02	0.149	0.0784	0.448
L-Zn²⁺ complex	$\tau_1 = 0.794$ $\tau_2 = 4.32$	$\beta_1 = 31$ $\beta_2 = 61.84$	1.95	1.09	0.047	0.0241	0.4887
L-Cd²⁺ complex	$\tau_1 = 0.628$ $\tau_2 = 3.81$	$\beta_1 = 28.04$ $\beta_2 = 70.96$	1.99	0.98	0.038	0.0191	0.4834
L-Hg²⁺ complex	$\tau_1 = 1.05$ $\tau_2 = 4.5$	$\beta_1 = 39.22$ $\beta_2 = 60.78$	1.96	0.98	0.024	0.0122	0.4979

We found that the “turn-off” band of **L** by Zn^{2+} at 316 nm was reversed by the addition of F^- and S^{2-} , although these anions did not cause any effects on the absorbance of free **L**. The ensembles **L-Cd²⁺** and **L-Hg²⁺** immediately entered a “turn-on” state by the addition of S^{2-} only. However, other anions (SO_4^{2-} , OAc^- , NO_3^- , F^- , Br^-) did not elicit any remarkable response in the absorbance of these complexes. As shown in ESI,† Fig. S23, upon treatment with 2 equiv. of S^{2-} , the reappearance of the absorption band at 316 nm implies the formation of $[\text{MY}_x]$ ($\text{M} = \text{Zn}^{2+}/\text{Cd}^{2+}/\text{Hg}^{2+}$ and $\text{Y} = \text{S}^{2-}$) from the **L-M²⁺** ensembles, freeing the ligand.²⁹ This “ON-OFF-ON” reversible cycle can be repeated several times (ESI,† Fig. S23a–c). Thus, the sensor can be chemically reset by S^{2-} , representing the reversibility.

Application in logic functions

The reversible and reusable switching process of **L** can be represented by a molecular logic gate by constructing two-input and two-output combinatorial logic circuits.³⁰ The logic circuit is planned with dual stimulant inputs of Hg^{2+} (In_1) and S^{2-} (In_2) and with the absorbances at 316 nm (OUT_1) and 394 nm (OUT_2) as the output modes. The threshold values of absorbance were set to be 1.01 and 0.32, respectively, for 316 nm and 394 nm. Absorbance lower than the threshold values have been assigned as “0”, and absorbances higher than the threshold values are considered as “1”, corresponding to the “off” and “on” states, respectively. There are four possible input combinations, (0, 0), (1, 0), (0, 1) and (1, 1), as shown in the truth table in Fig. 10b. In the absence of ions (considering the input signal “0, 0”, or no input) or in the presence of only S^{2-} (In_2 is ‘1’ and In_1 is ‘0’), OUT_1 at 316 nm is switched “on” (output signal “1”). Upon interaction with only Hg^{2+} , *i.e.*, In_1 is ‘1’ and In_2 is ‘0’, the absorbance at OUT_1 enters the “off” state (“0”). When both the inputs are present together (input signal “1–1”), the system regained the initial absorbance at 316 nm implying the “on” state (“1”). These combinations led to the construction of an “IMPLICATION” logic gate. However, in the absence of both inputs (Hg^{2+} or S^{2-}) and in the presence of only S^{2-} (In_2), the absorbance at 394 nm (OUT_2) was very low, which indicates the “off” state (output signal “0”) of the system. However, in the presence of only Hg^{2+} (In_1), a significant enhancement of the absorbance was observed, implying that OUT_2 enters the “on” state (“1”). These combinations represent the construction of an “INHIBIT” logic gate. The IMPLICATION logic function output is just complementary to an INHIBIT logic function and is closely related to the “if-then” phrase.³¹

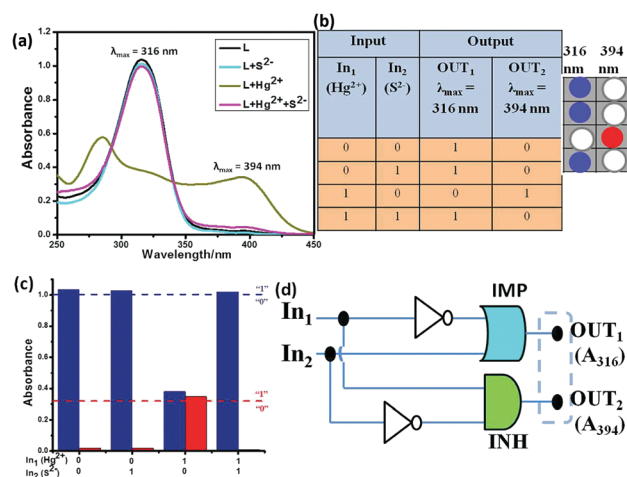


Fig. 10 (a) Output signals of the logic gate in the presence of different inputs, (b) corresponding truth table of the logic gate, (c) corresponding bar diagram of the absorbance outputs of **L** at $\lambda_{\text{max}} = 316 \text{ nm}$ (OUT_1 , blue bars) and $\lambda_{\text{max}} = 394 \text{ nm}$ (OUT_2 , red bars) in the presence of two inputs (Hg^{2+} and S^{2-}), (d) representation of the IMP/INH two-input and two-output-based logic circuit. Dotted lines indicate the threshold levels of the absorbance outputs.

Consequently, both the complementary IMP/INH logic functions can be performed in parallel at one time by the sensor **L** (Fig. 10d).

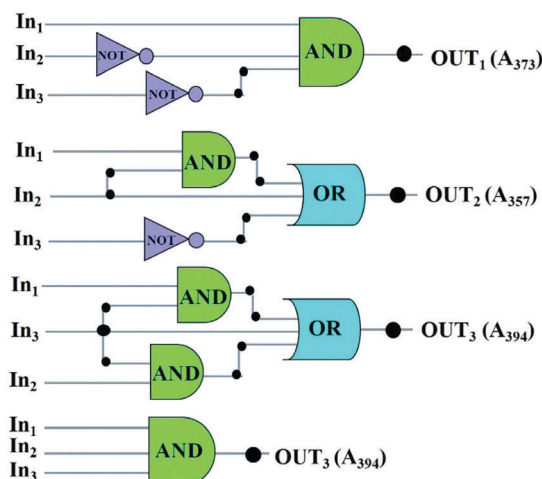


Fig. 11 Logic gate diagram for simultaneous monitoring of Zn^{2+} , Cd^{2+} and Hg^{2+} using **L**.

Table 4 Truth table for all plausible strings of input data and the corresponding output digits

Input			Output		
In ₁ (Zn ²⁺)	In ₂ (Cd ²⁺)	In ₃ (Hg ²⁺)	OUT ₁ λ _{max} = 373 nm	OUT ₂ λ _{max} = 357 nm	OUT ₃ λ _{max} = 394 nm
1	0	0	1	0	0
0	1	0	0	1	0
0	0	1	0	0	1
1	1	0	0	1	0
1	0	1	0	0	1
0	1	1	0	0	1
1	1	1	0	0	1

Furthermore, the set-reset of **L** was also explained by Zn²⁺ and S²⁻ and also by Cd²⁺ and S²⁻. In the case of the inputs Zn²⁺ and S²⁻, the absorbances at 316 nm and 373 nm were used as OUT₁ and OUT₂, respectively (ESI,† Fig. S24). Again, when Cd²⁺ and S²⁻ were chosen as inputs, OUT₁ and OUT₂ were at 316 nm and 357 nm, respectively (ESI,† Fig. S25). These outputs also generated combinatorial IMP/INH logic circuits.

Further, the selectivity of probe **L** between Zn²⁺, Cd²⁺ and Hg²⁺ was verified *via* a sequential logic circuit with three inputs, *viz.*, Zn²⁺ (In₁), Cd²⁺ (In₂), and Hg²⁺ (In₃), and three “turn-on” output signals of absorbance at λ_{max} = 373 nm (OUT₁ due to Zn²⁺), 357 nm (OUT₂ due to Cd²⁺) and 394 nm (OUT₃ due to Hg²⁺) (Fig. 11). All the input and output data are clearly represented in Table 4. A combination of AND, OR and NOT logic functions was used. When any one of the three inputs (Zn²⁺/Cd²⁺/Hg²⁺) was present, the corresponding output signal (at λ_{max} = 373 nm, 357 nm or 394 nm) became high (“1”), indicating the “ON” state. Thus, an OR logic gate could be generated. Again, when all three inputs were high (“1”), only the output signal at 394 nm (OUT₃) due to Hg²⁺ was observed and the signals for Zn²⁺ or Cd²⁺ were not observed, resulting in a NOT logic gate. This observation can be explained by the preference of **L** for complexation with Hg²⁺ even in the presence of Zn²⁺ and Cd²⁺. All these results clearly elucidate that this sensor can simultaneously or separately detect multiple ions by using appropriate outputs.

Conclusions

To sum up, a new simple 3-in-1 multi-response chemosensor **L** has been synthesized based on the pyrene group as a signaling unit and pyridine thiosemicarbazone as a chelator for selective recognition of the most familiar and abundant group 12 metal ions, *viz.*, Zn²⁺, Cd²⁺ and Hg²⁺. The sensor **L** not only exhibited sensitivity towards Zn²⁺, Cd²⁺ and Hg²⁺ due to heavy metal effects but also possessed distinct spectrophotometric and fluorimetric responses towards these ions. The selectivity response was found to follow the order of Hg²⁺, Cd²⁺, Zn²⁺ due to the different stability constants of their respective complexes. The selectivity was manifested by absorption spectra, interference studies and TDDFT calculations. The absorption intensities of the corresponding metal-ligand complexes could effectively be recycled several times by addition of S²⁻. The potential application of the probe for the construction of logic gates has been elaborated by using different chemical inputs and different

absorbances as outputs. All the results clearly elucidated that the chemosensor **L** provides a new approach for the detection of the most familiar and abundant group 12 metal ions simultaneously or separately.

Conflicts of interest

There are no conflicts to declare.

Acknowledgements

The authors thankfully acknowledge DST-FIST (SR/FST/CSI-267/2015 (C)) and NIT Durgapur for creating and providing infrastructural facilities for research. The authors are thankful to Visva-Bharati University for the ¹H NMR spectra and IACS, Kolkata for the ESI-mass spectra.

Notes and references

- 1 S. M. Z. Hossain and J. D. Brennan, *Anal. Chem.*, 2011, **83**, 8772–8778.
- 2 (a) H. Zhu, J. Fan, B. Wang and X. Peng, *Chem. Soc. Rev.*, 2015, **44**, 4337–4366; (b) M.-Q. Wang, K. Li, J.-T. Hou, M.-Y. Wu, Z. Huang and X.-Q. Yu, *J. Org. Chem.*, 2012, **77**, 8350–8354.
- 3 (a) J. M. Berg and Y. Shi, *Science*, 1996, **271**, 1081–1085; (b) B. L. Vallee and K. H. Falchuk, *Physiol. Rev.*, 1993, **73**, 79–118; (c) K. H. Falchuk, *Mol. Cell. Biochem.*, 1998, **188**, 41–48; (d) Z. Xu, J. Yoon and D. R. Spring, *Chem. Soc. Rev.*, 2010, **39**, 1996–2006; (e) H. Dai, Y. Yan, Y. Guo, L. Fan, Z. Che and H. Xu, *Chem. – Eur. J.*, 2012, **18**, 11188–11191.
- 4 (a) S. Kury, B. Dreno, S. Bezieau, S. Giraudet, M. Kharfi, R. Kamoun and J. P. Moisan, *Nat. Genet.*, 2002, **31**, 239–240; (b) E. Ho, *J. Nutr. Biochem.*, 2004, **15**, 572–578.
- 5 (a) J. Y. Koh, S. W. Suh, B. J. Gwag, Y. Y. He, C. Y. Hsu and D. W. Choi, *Science*, 1996, **272**, 1013–1016; (b) C. F. Walker and R. E. Black, *Annu. Rev. Nutr.*, 2004, **24**, 255–275; (c) M. P. Cuajungco and G. J. Lees, *Neurobiol. Dis.*, 1997, **4**, 137–169; (d) J. L. Smith, S. Xiong, W. R. Markesbery and M. A. Lovell, *Neuroscience*, 2006, **140**, 879–888; (e) P. Jiang and Z. Guo, *Coord. Chem. Rev.*, 2004, **248**, 205–229.
- 6 Agency for Toxic Substances and Disease Registry, 4770 Buford Hwy NE, Atlanta, GA 30341, <http://www.atsdr.cdc.gov/cercla/07list.html>.

- 7 (a) G. F. Nordberg, R. F. M. Herber and L. Alessio, *Cadmium in the Human Environment: Toxicity and Carcinogenicity*, Oxford University Press, Oxford, UK, 1992; (b) R. E. Hamon, M. J. McLaughlin, R. Naidu and R. Correll, *Environ. Sci. Technol.*, 1998, **32**, 3699–3703.
- 8 (a) G. Jiang, L. Xu, S. Song, C. Zhu, Q. Wu, L. Zhang and L. Wu, *Toxicology*, 2008, **244**, 49–55; (b) M. P. Waalkes, *J. Inorg. Biochem.*, 2000, **79**, 241–244; (c) W. de Vries, P. F. Romkens and G. Schutze, *Rev. Environ. Contam. Toxicol.*, 2007, **191**, 91–130; (d) H. N. Kim, W. X. Ren, J. S. Kim and J. Yoon, *Chem. Soc. Rev.*, 2012, **41**, 3210–3244.
- 9 (a) A. Franzblau, H. d'Arcy, M. B. Ishak, R. A. Werner, B. W. Gillespie, J. W. Albers, C. Hamann, S. E. Gruninger, H.-N. Chou and D. M. Meyer, *NeuroToxicology*, 2012, **33**, 299–306; (b) W. Y. Wong, *Coord. Chem. Rev.*, 2007, **251**, 2400–2427.
- 10 (a) T. W. Clarkson and L. Magos, *Crit. Rev. Toxicol.*, 2006, **36**, 609–662; (b) P. Mahato, S. Saha, P. Das, H. Agarwal and A. Das, *RSC Adv.*, 2014, **4**, 36140–36174.
- 11 (a) Q. Wang, D. Kim, D. D. Dionysiou, G. A. Sorial and D. Timberlake, *Environ. Pollut.*, 2004, **131**, 323–336; (b) P. B. Tchounwou, W. K. Ayensu, N. Ninashvili and D. Sutton, *Environ. Toxicol.*, 2003, **18**, 149–175; (c) M. Harada, *Crit. Rev. Toxicol.*, 1995, **25**, 1–24.
- 12 S. Pal, N. Chatterjee and P. K. Bharadwaj, *RSC Adv.*, 2014, **4**, 26585–26620.
- 13 (a) A. Sikdar, S. Roy, K. Haldar, S. Sarkar and S. S. Panja, *J. Fluoresc.*, 2013, **23**, 495–501; (b) Z. Liu, W. He and Z. Guo, *Chem. Soc. Rev.*, 2013, **42**, 1568–1600.
- 14 (a) J. H. Hu, Y. Sun, J. Qi, P. X. Pei, Q. Lin and Y. M. Zhang, *RSC Adv.*, 2016, **6**, 100401; (b) L. Yang, C. Wang, G. Chang and X. Ren, *Sens. Actuators, B*, 2017, **240**, 212–219; (c) K. B. Kim, H. Kim, E. J. Song, S. Kim, I. Noh and C. Kim, *Dalton Trans.*, 2013, **42**, 16569–16577; (d) A. Ghorai, J. Mondal, R. Saha, S. Bhattacharya and G. K. Patra, *Anal. Methods*, 2016, **8**, 2032–2040; (e) L. Chen, S. Y. Yin, M. Pan, K. Wu, H. P. Wang, Y. N. Fana and C. Y. Su, *J. Mater. Chem. C*, 2016, **4**, 6962–6966; (f) C. H. Min, S. Na, J. E. Shin, J. K. Kim, T. G. Jo and C. Kim, *New J. Chem.*, 2017, **41**, 3991–3999.
- 15 (a) S. Paul, S. Goswami and A. Manna, *Dalton Trans.*, 2015, **44**, 11805–11810; (b) R. Alam, R. Bhowmick, A. S. M. Islam, A. Katarkar, K. Chaudhuri and M. Ali, *New J. Chem.*, 2017, **41**, 8359–8369; (c) Y. Xu, D. Zhang, B. Li, Y. Zhang, S. Sun and Y. Pang, *RSC Adv.*, 2014, **4**, 11634–11639; (d) J. Sun, B. Ye, G. Xia and H. Wang, *Sens. Actuators, B*, 2017, **249**, 386–394.
- 16 (a) S. Samanta, U. Manna, T. Raya and G. Das, *Dalton Trans.*, 2015, **44**, 18902–18910; (b) W. Radchatawedchakoon, W. Sangsuwan, S. Kruanetr and U. Sakee, *Spectrochim. Acta, Part A*, 2014, **121**, 306–312; (c) D. Udhayakumari and S. Velmathi, *Sens. Actuators, B*, 2015, **209**, 462–469; (d) Y. W. Sie, C. F. Wan and A. T. Wu, *RSC Adv.*, 2017, **7**, 2460–2465; (e) S. Suganya, D. Udhayakumari and S. Velmathi, *Anal. Meth.*, 2013, **5**, 4179–4183; (f) Q. Ruan, L. Mu, X. Zeng, J.-L. Zhao, L. Zeng, Z.-M. Chen, C. Yang, G. Wei and C. Redshawd, *Dalton Trans.*, 2018, **47**, 3674–3678.
- 17 S. Mylonas and A. Mamalis, *J. Heterocycl. Chem.*, 2005, **42**, 1273–1281.
- 18 (a) H. D. Patel, S. M. Divatia and E. Clercq, *Indian J. Chem., Sect. B: Org. Chem. Incl. Med. Chem.*, 2013, **52**, 535–545; (b) D. Udhayakumari, S. Suganya and S. Velmathi, *J. Lumin.*, 2013, **141**, 48–52; (c) D. Udhayakumari, S. Velmathi, W. C. Chen and S. P. Wu, *Sens. Actuators, B*, 2014, **204**, 375–381.
- 19 (a) S. Sarkar, S. Roy, A. Sikdar, R. N. Saha and S. S. Panja, *Analyst*, 2013, **138**, 7119–7126; (b) S. Sarkar, S. Roy, R. N. Saha and S. S. Panja, *J. Fluoresc.*, 2018, **28**, 427–437; (c) B. Naskar, A. Dhara, R. Modak, D. K. Maiti, C. Prodhon, K. Chaudhuri, A. Requena, J. P. Cerón-Carrasco and S. Goswami, *ChemistrySelect*, 2017, **2**, 2512–2519; (d) K. Velmurugan, A. Raman, S. Easwaramoorthi and R. Nandhakumar, *RSC Adv.*, 2014, **4**, 35284–35289; (e) Y. Cho, S. K. Lee, J. W. Lee, S. Ahn and S. K. Chang, *Tetrahedron Lett.*, 2013, **54**, 5341–5344; (f) T. Raj, P. Saluja and N. Singh, *Sens. Actuators, B*, 2015, **206**, 98–106; (g) A. Ghosh, A. Sengupta, A. Chattopadhyay and D. Das, *Chem. Commun.*, 2015, **51**, 11455–11458.
- 20 (a) A. P. de silva, H. Q. N. Gunaratne and C. P. McCoy, *Nature*, 1993, **364**, 42–44; (b) A. Credi, V. Balzani, S. J. Langford and J. F. Stoddart, *J. Am. Chem. Soc.*, 1997, **119**, 2679–2681; (c) A. P. de Silva, H. Q. N. Gunaratne and G. E. M. Maguire, *J. Chem. Soc., Chem. Commun.*, 1994, 1213–1214; (d) K. Szacilowski, *Chem. Rev.*, 2008, **108**, 3481–3548; (e) X. Zhou, X. Wu and J. Yoon, *Chem. Commun.*, 2015, **51**, 111–113.
- 21 (a) P. Mahato, S. Saha and A. Das, *J. Phys. Chem. C*, 2012, **116**, 17448–17457; (b) N. Roy, S. Nath, A. Dutta, P. Mondal, P. C. Paul and T. S. Singh, *RSC Adv.*, 2016, **6**, 63837–63847.
- 22 (a) M. Shellaiah, Y. H. Wu, A. Singh, M. V. R. Raju and H. C. Lin, *J. Mater. Chem. A*, 2013, **1**, 1310–1318; (b) A. R. Chowdhury, P. Ghosh, B. G. Roy, S. K. Mukhopadhyay, N. C. Murmu and P. Banerjee, *Sens. Actuators, B*, 2015, **220**, 347–355; (c) A. Banerjee, A. Sahana, S. Das, S. Lohar, B. Sarkar, S. K. Mukhopadhyay, J. S. Matalobos and D. Das, *Dalton Trans.*, 2013, **42**, 16387–16395; (d) L. Wang, W. Qin and W. Liu, *Inorg. Chem. Commun.*, 2010, **13**, 1122–1125.
- 23 J. R. Lakowicz, *Principle of Fluorescence Spectroscopy*, Plenum, New York, 2006.
- 24 (a) P. Vishnoi, S. Sen, G. N. Patwari and R. Murugavel, *New J. Chem.*, 2015, **39**, 886–892; (b) N. Roy, S. Nath, A. Dutta, P. Mondal, P. C. Paul and T. S. Singh, *RSC Adv.*, 2016, **6**, 63837–63847; (c) R. V. Rathod, S. Bera, M. Singh and D. Mondal, *RSC Adv.*, 2016, **6**, 34608–34615; (d) S. P. Pawar, L. S. Walekar, U. R. Kondekar, D. B. Gunjal, A. H. Gore, P. V. Anbhule, S. R. Patil and G. B. Kolekar, *Anal. Methods*, 2016, **8**, 6512–6519.
- 25 (a) M. Royzen, Z. Dai and J. W. Canary, *J. Am. Chem. Soc.*, 2005, **127**, 1612–1613; (b) D. Maity and T. Govindaraju, *Chem. Commun.*, 2012, **48**, 1039–1041; (c) M. Shellaiah, Y.-H. Wu and H.-C. Lin, *Analyst*, 2013, **138**, 2931–2942.
- 26 H. A. Benesi and J. H. Hildebrand, *J. Am. Chem. Soc.*, 1949, **71**, 2703–2707.
- 27 R. H. Yang, W. H. Chan, A. W. M. Lee, P. F. Xia, H. K. Zhang and K. Li, *J. Am. Chem. Soc.*, 2003, **125**, 2884–2885.

- 28 (a) Y. Hong, J. W. Y. Lam and B. Z. Tang, *Chem. Soc. Rev.*, 2011, **40**, 5361–5388; (b) M. Shellaiah, T. Simon, V. Srinivasadesikan, C. M. Lin, K. W. Sun, F. H. Ko, M. C. Lin and H. C. Lin, *J. Mater. Chem. C*, 2016, **4**, 2056–2071; (c) N. Tripathi, P. Singh and S. Kumar, *New J. Chem.*, 2017, **41**, 8739–8747.
- 29 A. K. Singh and R. Nagarajan, *Dalton Trans.*, 2015, **44**, 19786–19790.
- 30 (a) H. Ding, C. Zheng, B. Li, G. Liu, S. Pu, D. Jia and Y. Zhou, *RSC Adv.*, 2016, **6**, 80723–80728; (b) K. Tayade, B. Bondhopadhyay, K. Keshav, S. K. Sahoo, A. Basu, J. Singh, N. Singh, D. T. Nehete and A. Kuwar, *Analyst*, 2016, **141**, 1814–1821; (c) T.-B. Wei, Y.-R. Zhu, H. Li, G.-T. Yan, Q. Lin, H. Yao and Y.-M. Zhang, *New J. Chem.*, 2016, **40**, 2327–2332; (d) D. Mondal, M. Bar, D. Maity and S. Baitalik, *J. Phys. Chem. C*, 2015, **119**(45), 25429–25441; (e) S. Wang, G. Men, L. Zhao, Q. Hou and S. Jiang, *Sens. Actuators, B*, 2010, **145**, 826–831.
- 31 S. Kumar, V. Luxami, R. Saini and D. Kaur, *Chem. Commun.*, 2009, 3044–3046.